Imaging the dissociation process of O_2 background gas during pulsed laser ablation of $LiNbO_3$

G. Epurescu,[a] J. Siegel,[b] J. Gonzalo, F. J. Gordillo-Vázquez, and C. N. Afonso
Laser Processing Group, Instituto de Óptica, CSIC, Serrano 121, 28006-Madrid, Spain

(Received 27 May 2005; accepted 28 September 2005; published online 16 November 2005)

The dynamics and the reactivity of the plasma produced during pulsed laser ablation of $LiNbO_3$ have been investigated. Optical emission spectroscopy combined with time-gated imaging with high spatial resolution is applied to the study of the factors that influence the plasma expansion process, the dynamics of the ejected species the influence of a background atmosphere (O_2 and Ar) and the reactivity of the expanding plasma. Direct evidence for O_2 dissociation occurring during expansion is presented and the temporal evolution of the spatial distribution of the dissociated O_2 is studied in detail. The influence of dissociation and velocities of the ablated species on the quality of thin films grown by pulsed laser deposition are discussed. © *2005 American Institute of Physics*.
[DOI: 10.1063/1.2135884]

Pulsed laser deposition offers superior abilities for growing complex oxide thin films that are stoichiometric and have good crystalline structure.[1,2] However, the processes that contribute to film deposition are still only partially understood, this being in part due to the large number of experimental deposition parameters involved. One key parameter is the background atmosphere. Its pressure and nature, reactive or inert, strongly influences the dynamics and the reactivity of the plasma due to the interaction between the ablated species and the background gas. An analysis of the ablation plasma provides a means to optimize the experimental parameters for thin film deposition. Several techniques have been applied to this purpose, including mass spectroscopy, ion probes, photography and imaging, optical emission spectroscopy, absorption spectroscopy, laser-induced fluorescence, etc. These plasma studies have mainly been focused to investigate the dynamics of individual species, the electron temperature and density, the ionization degree, etc.[1,3,4] Optical emission spectroscopy combined with time-resolved imaging provides enhanced measurement precision due to parallel acquisition of the spatial distributions of different species,[5,6] thus offering the possibility of recording simultaneously the expansion dynamics of all species ejected. This technique has the ability to visualize and precisely quantify the expansion dynamics and the fundamental parameters of the plasma produced during pulsed laser deposition.

In this letter we aim to use this technique to clarify the role of the background gas in the plasma expansion process during pulsed laser ablation of lithium niobate ($LiNbO_3$). In the case of an O_2 background, the possible dissociation of the oxygen molecules and the formation of oxides during plasma expansion have been proposed as a means to preserve the target stoichiometry in the film by enhancing the incorporation of oxygen.[7] Previous studies reported that a pressure of approximately 1 mbar of background gas, either O_2 or Ar, is required to obtain good quality stoichiometric $LiNbO_3$ films.[8,9] The occurrence of dissociation is, however, still under debate in the case of $LiNbO_3$ films and has not been addressed in Refs. 8 and 9. In this work the spatial distributions of the emitting species (Li^*, Nb^*, and O^*) of the laser-induced plasma in O_2 and Ar background pressures at different stages of the expansion process have simultaneously been recorded. A detailed analysis of the data shows important differences when using O_2 and Ar in terms of reactivity and dynamics.

The experimental setup is shown in Fig. 1(a). An ArF excimer laser ($\lambda = 193$ nm, pulse duration 20 ns) is focused (1.2 J/cm^2 laser fluence) on a $LiNbO_3$ single crystal target located inside a deposition chamber. The plasma produced that expands along the perpendicular to the target surface (z direction) is imaged onto a Czerny-Turner imaging spectrograph (25 cm focal length, 0.15 nm resolution) via two quartz lenses ($f_1 = 160$ mm, $f_2 = 100$ mm) and a periscope made of two aluminium mirrors. The purpose of the periscope is to rotate the plasma image by 90° such that the expansion direction lies along the entrance slit of the spectrograph. A 475 nm long-pass filter is used to block second order diffraction of shorter wavelength light. The output of the spectrograph is a one-dimensional (1D)-spatial and 1D-spectral image of the expanding plasma. It is recorded with a 16 bit time-gated ICCD camera (512×512 pixels) an example is shown in Fig. 2(b). In this image the vertical axis corresponds to the expansion direction z (1 pixel=28μm)

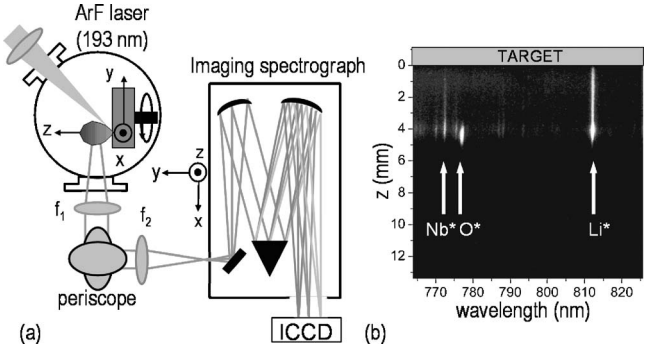

FIG. 1. (a) Experimental setup. (b) Example of a time-gated spatial-spectral image using a gate width of 100 ns and a delay of 400 ns with respect to the laser pulse. The arrows indicate the three emission lines studied in this work.

[a]On leave from: National Institute for Lasers, Plasma and Radiation Physics, 409 Atomistilor, 77125 Bucharest, Romania; electronic mail: epurescu@io.cfmac.csic.es
[b]Electronic mail: j.siegel@io.cfmac.csic.es

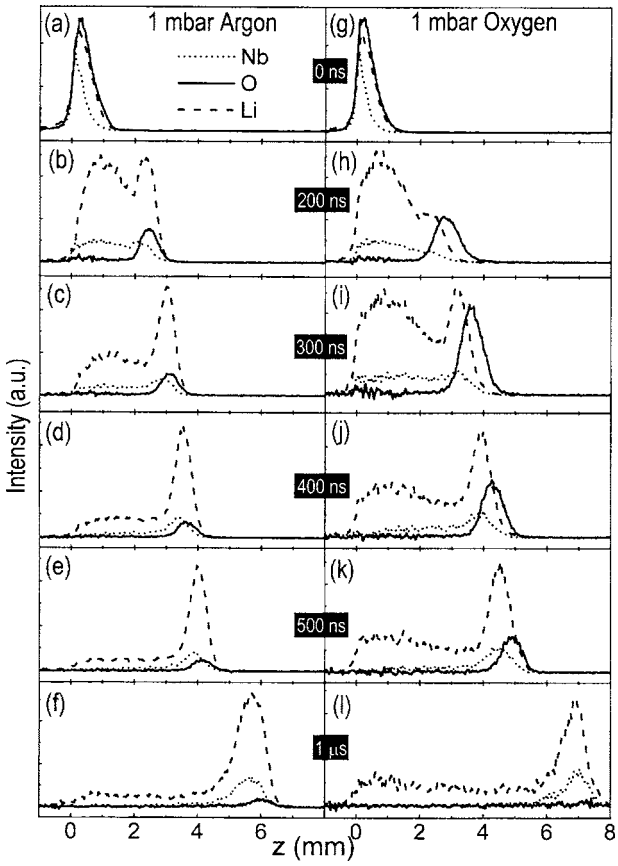

FIG. 2. Evolution of the spatial distributions of Li^* 812.6 nm (dashed line), Nb^* 773.6 nm (dotted line), and O^* 777 nm (solid line) in 1 mbar Ar and 1 mbar O_2 atmospheres. The different time delays are indicated in the figure. The distributions have been extracted from time-gated spatial-spectral images like the one shown in Fig. 1. The vertical axis of each frame has been scaled according to the intensity of the corresponding Li^* distribution of that frame.

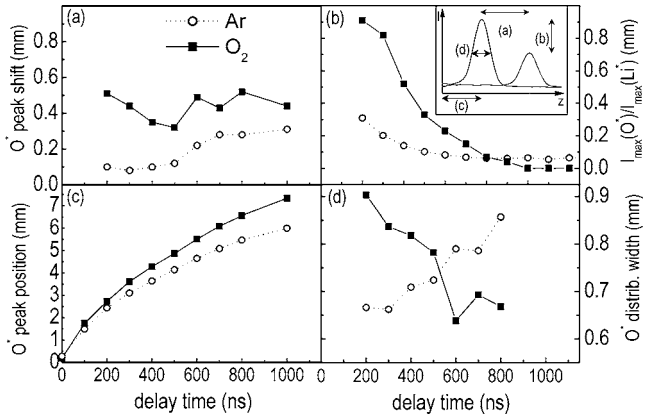

FIG. 3. Characteristic parameters of the spatial distributions in 1 mbar O_2 and 1 mbar Ar atmospheres as a function of delay time, extracted from data like those shown in Fig. 2: (a) Spatial shift of the O^* emission peak with respect to the Li^* emission peak. (b) Peak intensity of the O^* emission normalized to the peak intensity of the Li^* emission. (c) Spatial position of the O^* emission peak. (d) FWHM of the O^* emission. The inset in (b) is a sketch of two schematic spatial distributions (Li^* to the left and O^* to the right) where the characteristic parameters plotted in (a)–(d) are illustrated.

and the horizontal axis to the wavelength λ (1 pixel=1.2Å) of the emission of the species. A delay generator is used to delay the time gate of the ICCD with respect to the laser pulse by a user-defined value. The synchronization, delay, gate width, and image acquisition are controlled via software. More details on the experimental setup can be found elsewere.[5]

A series of time-gated spatial-spectral images have been recorded using a gate width of 100 ns and the delay was varied in steps of 100 ns up to 3 μs. Each image consists of ten accumulations covering a spectral interval of 62 nm (764–826 nm) and has been background subtracted. The plasma emission lines contained in these images correspond mainly to radiative transitions of excited neutrals. For this study we have selected the following lines: Nb^* 772.6 nm ($5p\ z^6P_{3/2} \rightarrow 4d^5a^6S_{5/2}$), O^* 777 nm ($3p^5P_{1,2,3} \rightarrow 3s^5S_2$) and Li^* 812.6 nm ($3s^2S_{1/2} \rightarrow 2p^2P_{1/2,3/2}$). Figure 1(b) shows a time-gated image of the expanding plasma in 1 mbar O_2, 400 ns after the laser pulse where the emission lines selected for this study are indicated by arrows. All distributions extend to a target distance of several millimeters and the signal intensity is higher at the distribution front due to the interaction between the species ejected from the target and the background gas. This effect, related to the shock wave produced at high pressure, increases the probability of excitations through collisions between the ablated species and the gas molecules at the shock wave front due to the higher density of atoms or molecules in this area.[3]

The transient spatial distributions of the emitting species have been extracted from each time-gated image by averaging over 13 pixel columns. The contribution from the electron continuous emission is removed by subtracting the signal collected at 784.7 nm (where there are no emission lines). In order to compensate for a spatially nonuniform sensitivity of the complete imaging system, caused by lens shading, nonuniform slit width, sensor amplification, etc., a shading correction was performed on all images. This correction essentially consists of dividing the image by a reference image obtained using a homogeneously illuminated white paper placed in the object plane, i.e., in the *X-Z* plane at the position of the plasma. In Fig. 2, these corrected spatial distributions are plotted for different delay times in both 1 mbar Ar [Figs. 2(a)–2(f)] and O_2 [Figs. 2(g)–2(l)] pressure. In Ar, directly after the laser pulse [delay=0 ns, Fig. 2(a)], single narrow distributions are observed for Li^*, Nb^*, and O^* close to the target surface (z=0 mm). The single distribution splits into two at a delay of 200 ns [Fig. 2(b)] in the case of Li^*. The first one consists of an intense and narrow peak caused by the interaction at the shock front and thus marks the boundary between the plasma region and background gas.[10] The second one is considerably broader and caused by the species ejected from the target at later times. As the delay is increased [Figs. 2(c)–2(f)], the first peak becomes dominant. A similar behavior is observed for Nb^*, although the relative contribution from the emission of the species ejected at later stages is considerably lower and virtually disappears at long delays [1 μs, Fig. 2(f)]. In the case of O^*, emission is only observed at the shock wave front for all delay times and no indications are found for delayed ejection.

In O_2 background gas [Figs. 2(g)–2(l)], the spatial distributions corresponding to Li^* and Nb^* and their evolution with increasing delays are similar to those observed in Ar. However, a very different evolution of the O^* distribution can by observed with respect to its position and intensity. As for the position, it is considerably advanced with respect to the first peaks of Li^* and Nb^*. This can more clearly be seen in Fig. 3(a), where the evolution of the spatial shift of the O^*

peak with respect to the Li^* peak in O_2 and Ar atmosphere has been plotted as a function of delay time. In Ar, this shift is negligible at early times and increases gradually. In O_2, the shift is larger at early times and decreases slightly up to a delay of ~500 ns before increasing again. The overall larger shift of O^* peak in O_2 atmosphere, particularly at the early stages of expansion, can be explained by an overlapped emission of O^* species ejected from the target and that of O^* from the background gas region. This additional contribution in O_2 atmosphere can also be appreciated in Fig. 3(b), showing the intensity of the O^* peak, normalized to the intensity of the first Li^* peak as a function of delay. At early times, in O_2, the O^* intensity is much higher than in Ar, suggesting the generation of additional O^* most likely through dissociation. The fact that fundamentally different processes occur in both gases is also apparent in Fig. 3(b) since O^* intensity decays down to zero within 1 μs in the case of O_2, whereas it decreases much more slowly to zero, (within approximately 2.5 μs) in the case of Ar.

The features observed in Figs. 2, 3(a), and 3(b) reveal the presence of a dissociation process of the O_2 molecules from the atmosphere at the leading edge of the shock front. Dissociation is possible because of the relatively low binding energy (5.12 eV) of O_2 and is caused by the collisions between O_2 molecules and the expanding plasma, leading also to excitation of the newly formed O atoms. While dissociation of O_2 has already been observed in earlier pulsed laser ablation experiments,[7,11–14] the technique used in the present study allows for the first time to precisely localize and simultaneously characterize the O^* distribution together with the distributions of the other excited neutral species involved, thus allowing a direct comparison of their relative positions and intensities. Moreover, this enhanced precision enables us to localize the dissociation process in space and time. Figure 3(c) shows the position of O^* peak as a function of time delay in both Ar and O_2 atmospheres and both curves show similar tendency to saturate in agreement with drag and shock-wave models. In contrast Camposeo *et al.*[13] reported two dissociation fronts, one showing a saturated tendency similar to our data and a second one, showing a linear increase, which they attributed to an additional contribution via collisions with ejected electrons. Since we do not observe such a linear component, the present results suggest that the collisions of the ejected atoms with the O_2 atmosphere have an important contribution to dissociation. Moreover, this hypothesis is further supported by the results presented in Ref. 14, attributing the presence of neutral oxygen to dissociation of molecular oxygen from the environment. However, we cannot completely exclude the contribution from collisions with energetic electrons present in the tail of the electron distribution function.

The full width at half maximum (FWHM) of the spatial O^* distribution, plotted in Fig. 3(d), provides supplementary information about the additional O^* contribution. At early times, the width in O_2 is up to 35% larger than in Ar due to the contribution from dissociation. For later times, the FWHM of the O^* distribution in O_2 becomes narrower as opposed to what happens in Ar. However, the behavior in Ar is the expected one due to collisions and different initial velocities. Additional studies are required to explain this phenomenon.

Despite the presence of additional atomic oxygen formed at the shock wave front upon dissociation of gas molecules in O_2, films grown in argon or oxygen in a previous work,[9] using the same experimental conditions and a target substrate distance of 30 mm, have been reported to be both stoichiometric, the crystalline quality being slightly better in the case of Ar. These results suggest that dissociation has no significant influence on the film stoichiometry. The role of the atmosphere is thus limited to defining the expansion dynamics in terms of divergence and velocity of the ejected species as suggested earlier.[9] Figure 3(c) shows that O^* species are slightly faster (approximately 20%) in O_2 than in Ar, for distances from the target up to 8 mm. Extrapolating this evolution to the substrate position at 30 mm using the drag and shock wave models, the velocity of the species reaching the substrate is expected to be lower in the case of Ar atmosphere. Since the velocity of the species arriving at the substrate surface strongly influences the mobility and surface damage,[15] a lower velocity as found in Ar appears to be beneficial for growing high quality crystalline thin films.

In conclusion, we have investigated the temporal and spatial evolution of the plasma produced by laser ablation of $LiNbO_3$, applying optical emission spectroscopy in combination with a time-gated imaging technique. The nature of the background atmosphere, inert (Ar) or reactive (O_2), is found to strongly influence the interaction of the atmosphere with the plasma in terms of expansion dynamics and reactivity. In O_2, dissociation of molecular oxygen from the atmosphere occurs at the boundary of the plasma region but only at early stages of plasma expansion. The high reactivity of atomic oxygen increases the possibility of oxides formation. However, the films deposited under the same experimental conditions in an earlier work (Ref. 9) are both stoichiometric, irrespective the gas nature. These observations suggest that while the gas pressure is responsible for maintaining the film stoichiometry, the lower velocity of the species observed in Ar can be responsible for the higher structural quality of those films.

This work was partially funded by CICYT (Spain), under Project No. TIC 2002-03235 and by European Union under Project No. HPRN-CT-2002-00328.

[1] *Pulsed Laser Deposition of Thin Films*, edited by D. B. Chrisey and G. K. Hubler (Wiley, New York, 1994).
[2] D. Bäuerle, *Laser Processing and Chemistry* (Springer, Berlin, 2000).
[3] D. B. Geohegan, Appl. Phys. Lett. **60**, 2732 (1992).
[4] S. S. Harilal, C. V. Bindhu, R. C. Isaac, V. P. N. Nampoori, and C. P. G. Vallabhan, J. Appl. Phys. **82**, 2140 (1997).
[5] J. Siegel, G. Epurescu, A. Perea, F. J. Gordillo-Vázquez, J. Gonzalo, and C. N. Afonso, Opt. Lett. **29**, 2228 (2004).
[6] E. M. Monge, C. Aragon, and J. A. Aguilera, Appl. Phys. A: Mater. Sci. Process. **69**, S691 (1999).
[7] A. Gupta, B. W. Hussey, and M. Y. Chern, Physica C **200**, 263 (1992).
[8] A. M. Marsh, S. D. Harkness, F. Quian, and R. K. Singh, Appl. Phys. Lett. **62**, 952 (1993).
[9] J. A. Chaos, J. Gonzalo, C. N. Afonso, J. Perrière, and M. T. Garcia-Gonzalez, Appl. Phys. A: Mater. Sci. Process. **72**, 705 (2001).
[10] K. R. Chen, J. N. Leboeuf, R. F. Wood, D. B. Geohegan, J. M. Donato, C. L. Liu, and A. A. Puretzky, Appl. Surf. Sci. **96-98**, 45 (1996).
[11] J. Hermann and C. Dutouquet, J. Phys. D **32**, 2707 (1999).
[12] X. Y. Chen, Z. C. Wu, Z. G. Liu, X. Y. Lei, and Z. S. Sha, Appl. Phys. A: Mater. Sci. Process. **67**, 331 (1998).
[13] A. Camposeo, F. Cervelli, F. Fuso, M. Allegrini, and E. Arimondo, Appl. Phys. Lett. **78**, 2402 (2001).
[14] F. Cervelli, F. Fuso, M. Allegrini, and E. Arimondo, Appl. Surf. Sci. **127-129**, 679 (1998).
[15] S. F. Xu, Y. J. Tian, H. S. Lu, D. F. Cui, Z. H. Chen, B. Li, and G. Z. Yang, Supercond. Sci. Technol. **7**, 435 (1994).